



LAWRENCE
LIVERMORE
NATIONAL
LABORATORY

HIGH-MODE RAYLEIGH-TAYLOR GROWTH IN NIF IGNITION CAPSULES

B. A. Hammel, S. W. Haan, D. Clark, M. J. Edwards, S.
H. Langer, M. Marinak, M. Patel, J. Salmonson, H. A.
Scott

August 10, 2009

Second International Conference on High Energy Density
Physics (ICHED2009)
Austin, TX, United States
May 19, 2009 through May 22, 2009

Disclaimer

This document was prepared as an account of work sponsored by an agency of the United States government. Neither the United States government nor Lawrence Livermore National Security, LLC, nor any of their employees makes any warranty, expressed or implied, or assumes any legal liability or responsibility for the accuracy, completeness, or usefulness of any information, apparatus, product, or process disclosed, or represents that its use would not infringe privately owned rights. Reference herein to any specific commercial product, process, or service by trade name, trademark, manufacturer, or otherwise does not necessarily constitute or imply its endorsement, recommendation, or favoring by the United States government or Lawrence Livermore National Security, LLC. The views and opinions of authors expressed herein do not necessarily state or reflect those of the United States government or Lawrence Livermore National Security, LLC, and shall not be used for advertising or product endorsement purposes.

High-mode Rayleigh-Taylor growth in NIF ignition capsules

B.A. Hammel, S. W. Haan, D. Clark, M. J. Edwards, S.H. Langer, M. Marinak, M. Patel, J. Salmonson, and H.A. Scott

Lawrence Livermore National Laboratory, Livermore CA, U.S.A.

Email: hammell@llnl.gov

Abstract: An assessment of short wavelength hydrodynamic stability is an essential component in the optimization of NIF ignition target designs. Using highly-resolved massively-parallel 2-D Hydra simulations [1], we routinely evaluate target designs up to mode numbers of 2000 ($\lambda \sim 2 \mu\text{m}$) [2]. On the outer ablator surface, mode numbers up to ~ 300 ($\lambda \sim 20 \mu\text{m}$) can have significant growth in CH capsule designs. At the internal fuel:ablator interface mode numbers up to ~ 2000 are important for both CH and Be designs. In addition, “isolated features” on the capsule, such as the “fill-tube” ($\sim 5 \mu\text{m}$ scale-length) and defects, can seed short wavelength growth at the ablation front and the fuel:ablator interface, leading to the injection of ~ 10 's ng of ablator material into the central hot-spot. We are developing methods to measure high-mode mix on NIF implosion experiments. X-ray spectroscopic methods are appealing since mix into the hot-spot will result in x-ray emission from the high-Z dopant (Cu or Ge) in the ablator material (Be or CH).

1. Introduction

Controlling the hydrodynamic growth of high-mode perturbations is an essential component of the optimization of NIF ignition target designs. A schematic of a typical ignition capsule is shown in Figure 1. On the outer ablator surface, mode numbers ($m = 2\pi r/\lambda$) up to ~ 300 ($\lambda \sim 20 \mu\text{m}$) can have significant growth, and are particularly important for assessing the impact of roughness on the surface of CH capsules where the dominant unstable mode in some designs is ~ 160 . At the internal fuel:ablator interface, where very short wavelength perturbations can grow at the steep gradients, mode numbers up to ~ 2000 ($\lambda \sim 2 \mu\text{m}$) are important [2]. In typical designs, roughness at this interface (inner ablator surface) leads to mixing of ablator material into the outer $\sim 30\%$ of the cold dense fuel mass. Finally, “isolated features” on the capsule, such as the “fill-tube” ($\sim 5 \mu\text{m}$ scale-length) and defects, can seed short wavelength growth at the ablation front and the fuel:ablator interface, leading to the injection of small amounts (~ 10 's ng) of ablator material into the central hot-spot. In general, we find that experimental conditions, such as the spectrum of the x-ray drive, and models for the physical data, such as material equation of state (compressibility) and thermal conductivity, are important as they influence the magnitude of the simulated high-mode growth. All simulations reported here are performed with HYDRA [1].

2. High mode number (~ 100) growth seeded on the outer capsule surface

For comparing designs it is useful to determine the linear growth factors (GF) *vs.* mode number at the important unstable interfaces. This can be achieved by performing a simulation of a capsule that includes a small Gaussian-shaped bump as a radial perturbation at the interface of interest. The GF *vs.* mode number is then determined by the ratio of the Legendre coefficients for the final and initial perturbations. In Figure 2a we show a comparison of the linear GF for typical Be and CH capsule designs (for two different models for the CH Equation of State (EOS)), where the initial perturbation is placed on the outer ablator surface, and the final perturbation at peak velocity is assessed at the fuel:ablator interface. CH shows higher growth than Be overall, and is significantly more unstable above mode ~100. Also, the QEOS model [3] for CH shows less growth than the LEOS model [3, 4].¹ This difference is apparent before the capsule begins to accelerate inwards, but after the shocks have travelled through the ablator and fuel, as seen in the growth factor in areal density shown in Figure 2b. The relative compressibility ($\rho_{\text{shocked}}/\rho_0$) of the materials is important here. For a typical 3-MB first shock, the compression on the principal Hugoniot for Be (LEOS-41) is 1.95, compared to 2.7 for CH-QEOS, and 2.9 for CH-LEOS. More compressible materials support higher mode perturbations in areal density, providing a larger seed for R-T growth once the capsule begins to accelerate. The same trend is seen in a more recent EOS model for CH (LEOS-5310), which is more compressible than LEOS-5101 (above 2 MB), and shows higher growth.

The effect of the different GF during the shock transit and implosion phases can be seen clearly in Figure 3 where we plot the fractional peak-to-valley (PTV) ρR variation *vs.* normalized implosion time resulting from a small Gaussian perturbation (+30 nm for CH and +40 nm for Be, both 12- μm FWHM). The final fractional PTV ρR variation for the Be capsule is a factor of ~30 smaller than for two variations of a CH design (“High Foot” and “Low Foot”).² As in Figure 2, this difference is apparent after the shock transit phase and before the capsule begins to accelerate (at normalized times 0.8 for Be and 0.85 for CH). In the implosion phase, the Rayleigh-Taylor growth factor for Be and CH is comparable.

The large GF for CH capsules sets stringent requirements for the outer surface smoothness. Isolated defects, which appear on the outer capsule surface as small mounds with diameters in the range of ~10-30- μm (significant power around mode 100), invert in sign (for negative GF) and can grow enough to penetrate the shell if their initial amplitude is too large. Simulations for a “High Foot” CH capsule design indicate that a single +400 nm (outward) amplitude Gaussian defect (15- μm FWHM) on the outer capsule surface (placed on the pole in the 2D simulations to approximate the 3D case), develops a jet that penetrates through the shell, introducing ~ 10 ng of ablator material into the hot-spot (Figure 4). This decreases to ~5 ng for a +300 nm perturbation. Simulations also indicate that changes in the strength of the first shock (*i.e.* the intensity of the “foot” of the laser pulse) modify the location of the zero in the growth factor as seen in Figure 5. As a consequence, a positive amplitude (outward going) isolated feature of this size results in a smaller final perturbation and no longer penetrates the shell. The reduced fractional ρR variation for the “Low Foot” drive case (for a small +30 nm bump) is apparent in Figure 3. Although a “Low Foot” drive reduces the impact of outward going bumps, it results in large positive GF near mode 100 (Figure 5). As a consequence, features with negative sign (inward “dimples”) grow more than in the “High Foot” case. Those with -300-nm amplitude grow enough to introduce ablator mass into the hot-spot.

The exact location of zeros in the GF are known to be sensitive to details in the simulations and in the physical data (*e.g.* EOS and opacity models), so the influence of the “foot height”

on the sign of the growth of should be interpreted with caution in any specific growth factor curve. For the envelope of the growth factor, other than phase issues, we estimate that there is a 40% uncertainty in the simulated perturbation amplitudes as a result of uncertainty in EOS models.

3. Very high mode number (~ 1000) growth at the fuel:ablator interface

For a perturbation at the interface between the ablator and the fuel, high-mode perturbations are not stabilized by ablation and can grow at the steep internal gradients. In the indirect-drive NIF target (Figure 1), the innermost region of the ablator is shielded from the drive x-rays by outer layers of ablator that are doped with varying amounts of high-Z material (Cu in the Be target or Ge in the CH target) [7]. The shielding reduces the heating of the innermost layer, keeping its density high so as to accelerate the dense DT with minimum instability growth. A profile of the density and temperature as a capsule approaches peak velocity is shown in Figure 6a. The difference in the heating of the Be and the relatively transparent DT is apparent in the rapid rise in the temperature across the interface. The DT fuel closest to the interface is heated by the hotter Be through thermal conduction, causing its density to drop, in order to maintain pressure balance. Similarly, the Be closest to the interface is cooled, and its density increases. The gradient scale-length for the DT and Be in the region of their interface is determined by the thermal conductivity in the two materials and is typically $\sim 1\text{-}3\ \mu\text{m}$. Wavelengths shorter than this scale-length (mode numbers > 1000) will be stabilized.

It is important to note that thermal conductivity models are uncertain in this regime ($\sim 10\ \text{g/cm}^3$, $\sim 10\text{-}30\ \text{eV}$), and not confirmed by experiment. This particular simulation used Lee-More conductivity[8]. The effect on the density profile from multiplying this conductivity by an arbitrary factor of 0.3 and 3.0 is shown in Figure 6b. In 2D simulations with a perturbation at the interface, we observe a corresponding change in final mix thickness as shown in Figure 7a, where the 0.3 \times case (shorter scale-length) exhibits more mix. We generally use Purgatorio conductivities [9] for our high mode simulations. This model is thought to be uncertain to about half the level over which we have varied the conductivity here, corresponding to an uncertainty in the mix width of $\sim 25\%$.

The high-mode perturbation growth shows evidence of the onset of saturation and non-linearity of the final mix amplitude with initial perturbation size. The perturbation PTV amplitude vs. time is plotted in Figure 7b (for the nominal Lee-More conductivity case), for two different initial amplitude multi-mode perturbations at the interface, nominal and 0.25 \times nominal. The PTV amplitudes maintain their 4 \times ratio until they reach a PTV of $\sim 3\ \mu\text{m}$, which is comparable to the dominant wavelength. By the time of peak velocity, the final amplitudes differ by only $\sim 2\times$. For the nominal amplitude case the PTV mix width for this capsule design is $\sim 30\%$ of the thickness of the DT fuel.

As the capsule decelerates, the perturbations that form at the boundary of the hot-spot are stabilized by the density gradient scale-length and ablation, and are limited to low modes (< 50) (Figure 8). For capsules that meet the requirements (“at-spec”)³ for surface smoothness on the inner surface, the perturbation growth does not result in high-mode perturbations penetrating the hot-spot. Capsules with “at spec” roughness on the inner and outer ablator surfaces, and the DT ice, including designs where ablator has mixed into the outer $\sim 50\%$ of the fuel, ignite and burn in the simulations.

High levels of fuel:ablator mix do adversely affect the robustness of the capsule, moving it closer to its “cliffs” - failing sooner with off-nominal conditions such as decreasing implosion velocity or increasing entropy. A typical capsule’s yield vs. fuel:ablator mix fraction (mix penetration of the fuel as a fraction of the fuel mass) is shown in Figure 9. For a case where the fuel has nominal velocity, entropy, and low-mode hot-spot perturbations, the capsule can tolerate ~50% mixing at the interface and still perform well (~ 10 MJ). However, for a case where the velocity, fuel entropy and hot-spot perturbation are all worse than their nominal values, each by $1\sigma/\sqrt{3}$, there is a faster decline in yield with mix.⁴ This is more pronounced for the third case plotted – the unlikely situation where the velocity, fuel entropy and hot-spot shape are each worse by 1σ on their respective uncertainties.

The principal method of controlling high-mode mixing at the fuel:ablator interface is to control the relative densities of the DT fuel and the ablator. This can be achieved by varying the amount of high-Z dopant in the ablator. The “fuel:ablator density ratio”, evaluated as the shell approaches peak velocity, is a useful figure of merit for characterizing the high mode stability at the interface. An example of the influence of dopant fraction on this density ratio and the resulting mix width is shown in Figure 10. By increasing the areal density of the dopant (Cu) by a factor of 1.4, the fuel:ablator density ratio (evaluated at the densities marked by the triangles in Figure 10a) changed from 1.4 to 1.1, and the mix width decreased from ~ 40% to less than 5%.⁵ Typically, increasing the level of ablator dopant to reduce the mix width by 50% requires a ~10% increase in laser energy to maintain the same implosion velocity. For this reason, most designs use a more moderate increase in the dopant concentration than the 1.4× used here. In our overall optimization we typically consider designs with a fuel:ablator density ratio less than 1.3, which limits the ablator mix to the outer ~30% of the fuel mass.⁶ The mix width vs. fuel:ablator density ratio is plotted in Figure 11 for a wide range of target designs.

The other factor that affects the fuel:ablator density ratio is the amount of ablator mass that remains when the capsule reaches peak velocity. Ablating away too much mass, from either a higher than expected mass ablation rate, or from excessive x-ray drive, will increase the fuel:ablator density ratio and the resulting mix. This effect can be seen in the 3 square points in Figure 11, where the same capsule design was driven with three different fluxes; nominal x-ray flux giving the highest amount of mix, and two reduced drive cases (0.96 and 0.83 multipliers on the peak flux) showing correspondingly less mix. If NIF implosion experiments show evidence of excessive fuel:ablator mix, then increasing the ablator thickness is another way to improve the stability. As with increasing the high-Z dopant, this would require additional laser energy to maintain a fixed implosion velocity.

Another source of uncertainty that influences the density of the fuel and ablator near their interface is the spectral dependence of the x-ray drive. The non-Planckian x-ray drive spectrum includes an energetic component (gold M-band emission) that is due primarily to the regions of the hohlraum plasma heated directly by the laser beams. Figure 12 shows two simulations of a relatively stable Be capsule (with higher Cu dopant than the design in Figure 6 to reduce high-mode mix), one driven with the nominal drive spectrum and the other with a “hardened spectrum”, where the driving x-ray flux for $h\nu > 1.8$ keV was increased in a time dependent fashion corresponding to our current estimate of the maximum plausible level. The hardened spectrum causes more preheat in the innermost undoped layer of ablator, causing its density to drop relative to the DT fuel. The degree of ablator mix penetration into the DT fuel is shown in Figure 11 (plotted as circles) for the two drive spectrum cases. In the nominal (hardened)

case, where the fuel:ablator density ratio is 1.21 (1.34), the outer 9% (28%) of the fuel mass contains $\geq 10\%$ Be by mass (Figure 12b). The drive spectrum will be measured in early NIF experiments, which will allow for re-optimization of the high-Z dopant fraction, as discussed above. There will be residual uncertainty in the mix width, related to the uncertainty in the measurement of the x-ray drive spectrum, which we estimate to be $\sim 25\%$.

The linear GF for a perturbation at the fuel:ablator interface can be determined from a simulation with a small Gaussian perturbation (0.5-nm amplitude, 3.5- μm FWHM), now placed initially on the inner surface of the capsule. The GF vs. mode number, for a Be capsule design with fuel:ablator density ratio of 1.32, is plotted in Figure 13. The high GF at mode numbers ~ 1000 sets stringent requirements for the inner surface smoothness of capsules and for the density uniformity of the ablator material. Simulations indicate that for this Be capsule design, a single +100-nm (outward) amplitude “isolated defect” (Gaussian bump, 15- μm FWHM) on the inner capsule surface, results in a jet that penetrates into the hot-spot.

Simulations also indicate that short wavelength variations in the density of the Be ablator material can seed significant growth at the fuel:ablator interface. The fabrication method for Be targets results in density variations on length scales of 50 nm – too small for direct simulation using our current methods. We have done simulations with an approximate model for the density fluctuations, with density variations that were 4- μm long radially, 0.7- μm wide, 0.6% deep, and sufficiently numerous to cause 0.08% RMS density variability. These cause a fractional ρR variation of 0.02% RMS, and result in Be mixing into the outer $\sim 45\%$ of the fuel mass. For comparison, “at-spec” roughness on the inner Be surface, for this same design, results in mixing into the outer 32% of the fuel mass. Experiments have been done measuring the shock velocity uniformity in Be. The measured shock is smoother than this simulation indicates for this density, so this is an overestimate of the expected mixing. Furthermore, the scale-length of the actual target fluctuations corresponds to mode numbers $\sim 10,000$ where viscous stabilization will be important. We are working to improve our modeling in this area.

4. 3D

Since actual measured surfaces of both Be and CH capsules contain small localized defects, an accurate assessment of their impact is important in our overall optimization of target designs. 2D simulations, with the defect placed on the “pole” (axis of symmetry), constrain the solution to be axially symmetric and limit the study to a single isolated bump. We have also performed highly resolved 3D HYDRA simulations ($4.5^\circ \times 4.5^\circ$ equatorial segment, resolving up to mode ~ 1000), using actual measured roughness for the inner and outer ablator surface, as shown in Figure 14. For this simulation (Be capsule), the inner surface was chosen to include a region with several $< 50\text{-nm}$ defects to assess their effect on the mix region. By peak velocity these features have grown enough to penetrate through 75% of the DT fuel, but not enough to inject mass into the hot spot. This will be addressed more thoroughly in future work.

5. Fill-tube or “isolated defect” mix

The capsule “fill-tube/fill hole” combination (Figure 15a) is an additional isolated defect that must be evaluated for each capsule design [10]. It forms a high-mode perturbation that can grow at both the ablation front and the fuel:ablator interface. In most designs that we have examined this perturbation introduces a minimum of ~ 10 ng of ablator material into the hot-spot. Although this amount of injected material is acceptable, degradation in capsule performance becomes significant at several times this amount. If the combined high mode growth at the ablation front and the fuel:ablator interface is too large, the long bubbles of ablator material, seen in the Region plot in Figure 15b, can reach further through the dense shell, increasing the mass in the hot-spot to unacceptable levels.

An assessment of the total amount of mass injected into the hot spot from the fill-tube and other isolated defects (such as those on CH capsules discussed above) is an important factor in our overall optimization of design robustness. We are developing methods to measure hot-spot mix on NIF capsule implosions in early experiments, before the start of the actual ignition shots, where the peak hot-spot electron temperatures will be relatively low (~ 2 - 3 keV). In the case of isolated defects on the outer surface of CH capsules, simulations indicate that most of the injected ablator mass is high-Z doped (Figure 4), resulting in a clear signature in the x-ray emission from the hot-spot. For a fill-tube perturbation the jet is generally a mixture of doped and undoped ablator.

Early experiments will include a campaign investigating the performance of capsules with “layered” cryogenic fuel [11]. Consistent with limits of early routine facility operation, the NIF laser pulse will be limited to power levels below that of the “ignition pulse shape” and the neutron yield will be limited by altering the composition of the fuel layer to $\sim 75\%$ T_2 : 25% H_2 , with a small amount of D_2 (this composition is referred to as “THD”) for nuclear diagnostic measurements. A simulation of a typical “High-Foot” CH THD capsule design is shown in Figure 16. This simulation included “NIF spec” roughness on the CH surfaces (inner and outer) and the fuel layer, but had an additional Gaussian bump added to the outer CH surface to form a $+300$ -nm amplitude, 20 - μ m wide “isolated defect” on the pole. The capsule was driven by a version of the ignition x-ray drive pulse shape that was reduced by a factor of 0.7 in the peak. The injected ablator mass, for this large defect case, is ~ 20 ng. In a simulated x-ray image (photon energy > 8 keV) of the compressed core the high-Z jet dominates the emission from the surrounding DT (Figure 17). A simulated x-ray spectrum, generated by using Cretin [12] to post-process a HYDRA time-dump, shows measurable levels of Ge K-shell emission (Figure 18), potentially providing a means to quantify the amount of mix and the electron density ($\sim 10^{25}$ cm^{-3}) and electron temperature (~ 2 keV) in the mixed regions.

6. Summary

An assessment of hydrodynamic growth at high mode numbers is essential in the optimization of ignition target designs. Growth on the outer ablator surface is particularly important for CH capsules, where isolated defects ~ 300 -nm amplitude can grow enough to inject ablator material into the hot-spot. At the internal fuel:ablator interface, very high modes grow at the steep gradients, and typically result in ablator material mixing in to the outer $\sim 30\%$ of the fuel. Isolated defects at this interface greater than ~ 100 -nm amplitude can also result in ablator material entering the hot spot. These conclusions have a degree of uncertainty due to uncertainties in experimental conditions, physical models and the simulation method itself.

Overall, we estimate there is a factor of 2 uncertainty in the simulated mix, and include this uncertainty in the overall evaluation of target designs.⁷

This work was completed under the auspices of the U.S. Department of Energy by Lawrence Livermore National Laboratory under Contract DE-AC52-07NA27344.

Figure 1. Schematic of a typical capsule. The inner bands of the ablator (CH or Be) are doped with a high-Z element (Ge or Cu). The outermost and innermost ablator regions are not doped. Typical dimensions are outer ablator radius: 1200 μm ; Inner ablator radius: 1000 μm . Specific dimensions for a current optimized CH target are outer radius : 1160 μm ; total ablator thickness: 200 μm ; fuel thickness: 63 μm ; innermost ablator layer (undoped): 5 μm ; 2nd layer (doped 0.2 % Ge): 5 μm ; 3rd layer (doped 0.5 % Ge): 39 μm ; 4th layer (doped 0.2 % Ge): 15 μm ; outermost layer (undoped): 136 μm . This capsule is contained in a hohlraum that is driven with 1.5 MJ of 3ω light, resulting in a peak drive temperature of 300 eV.

Figure 2. a) Growth Factor at peak velocity for a radial perturbation at the fuel:ablator interface, resulting from a small amplitude Gaussian perturbation (12- μm FWHM) that was initially on outer ablator surface of a CH and Be capsule; b) GF in areal density for the same perturbation, after shock transit and before acceleration. More compressible materials result in more high-mode growth. The x-ray drive was a “high-foot” design. The 2-D simulations covered a 22.5° segment of the capsule that includes the pole (axis of symmetry), therefore mode numbers below ~ 10 are not accurately represented.

Figure 3. Fractional peak-to-valley areal density $\rho R(PTV)/\langle\rho R\rangle$ vs. normalized implosion time, for a Be capsule and two versions of a CH design; Strong first shock (“High Foot”) and low first shock (“Low Foot”). Initial Gaussian perturbation was 12- μm FWHM, amplitude +30 nm for CH and +40 nm for Be. In “Low Foot” case, x-ray flux in the foot (resulting from the initial “picket” in the laser pulse) was lower than “High Foot” case by a factor of 0.48, and the rest of the pulse was identical, but delayed by 1.7 ns. Both the “High-Foot” and “Low-Foot” CH designs use LEOS-5105.

Figure 4. (a) Density and Material Region plot, at a time (18 ns) near peak implosion velocity, for a CH capsule with a +400-nm amplitude, 15- μm FWHM Gaussian “isolated defect” on the outer ablator surface (placed on the pole), showing CH ablator material has penetrated the imploding shell. (b) Integrated mass (g) vs. radius (cm) showing DT mass (dot: initially gas, dash: initially ice, solid: all DT) and ablator mass (dash: Ge doped CH, solid: all CH). Approximately 10 ng of CH has penetrated the imploding shell (< 0.014 cm radius) at this time, and most of it is Ge-doped.

Figure 5. Growth Factors vs. mode number for two versions of a CH design; Strong first shock (“High Foot”) and low first shock (“Low Foot”). In “Low Foot” case, x-ray flux in the foot (resulting from the initial “picket” in the laser pulse) was lower than “High Foot” case by a factor of 0.48, and the rest of the pulse was identical, but delayed by 1.7 ns.

Figure 6. a) Radial profile during the implosion of a Be capsule, as it approaches peak velocity (14.4 ns), of the density (g/cc) and temperature (eV); b) Variation in the profiles for 0.3 (dot), 1.0 (solid), and 3.0 (dash) times the nominal thermal conductivity (Lee-More) [8]. In this simulation, initial roughness at the fuel:ablator interface is a multimode perturbation including mode numbers (l) up to $l=1000$.

Figure 7. (a) Simulation of mix at the interface for the three conductivity cases, near peak velocity. (b) PTV amplitude vs. time for nominal and 0.25×nominal initial amplitude. The vertical lines between the curves indicate a factor of 4.

Figure 8. Growth on the hot-spot perimeter for a Be capsule with roughness on the inner and outer ablator surfaces, and on the DT fuel, just before ignition. The hot-spot perturbation is limited to modes < 50 by scale-length and ablative stabilization. RHS is a pseudocolor plot of density. LHS shows material regions.

Figure 9. A typical capsule's yield vs. mix penetration of the fuel as a fraction of the total fuel mass, for nominal and off-nominal experimental conditions. Solid - nominal velocity, entropy, and low-mode hot-spot perturbations; Dash - velocity, fuel entropy and hot-spot perturbation are all worse than their nominal values, each by $1\sigma/\sqrt{3}$; Dot - velocity, fuel entropy and hot-spot shape are each worse by 1σ on their respective uncertainties.

Figure 10. (a) The effect of increasing the areal density of the dopant by 1.4× on the density and temperature profiles (solid is nominal dopant, dashed is higher dopant). Triangles mark the location where the fuel:ablator density ratio is evaluated for the nominal dopant case. (b) Pseudocolor plots of the density of the imploding shell in the region of the interface, showing the reduction in mix width going from nominal dopant (upper) to higher dopant (lower).

Figure 11. Mix width vs. fuel:ablator density ratio over a wide range of target designs. Mix width is defined as the fraction of fuel mass that contains $\geq 10\%$ ablator by mass. The three square points correspond to one capsule design for three different drive conditions: nominal, 0.96 and 0.83 multiplier on the peak of the drive (x-ray flux). The two circles are for a design with a nominal and “hardened spectrum”.

Figure 12. (a) Pseudocolor plot of density of imploding shell showing mix in the region of the fuel:ablator interface for the Nominal drive spectrum (top) and the Hardened drive spectrum (bottom). (b) Mix fraction vs. fuel mass as a fraction of the total fuel mass (Normalized Fuel Mass) for the two cases, showing increase from 9% to 28% mix with Hardened drive spectrum. Time dependent multipliers for the “hardened” case were 3× (0 – 2 ns), 2× (5 ns), 1.6× (7 – 10 ns), 1.3× (15 – 18 ns).

Figure 13. Growth Factors vs. mode number for a perturbation on the inside surface of a Be capsule, for a design with fuel:ablator density ratio 1.32.

Figure 14. Pseudocolor plot of density from a 3D simulation of a Be target with measured roughness on inner and outer Be surfaces.

Figure 15. (a) Typical configuration for 2D simulation of the fill-tube and fill-hole for a CH ignition capsule. Tube dimensions: 10- μm OD, 5- μm ID, 40- μm counter bore depth. Hole

diameter: 5 μm . The axis of symmetry is vertical, and the simulation covered 45° (b) Density and Region plots near peak compression, showing 20 ng of ablator material that has entered the hot-spot.

Figure 16. Density and Material Region plot, at a time approaching peak compression, for a CH THD capsule. This simulation included “NIF spec” roughness on the CH surfaces (inner and outer) and the fuel layer, but had an additional Gaussian bump added to the outer CH surface to form a +300 nm amplitude, 20- μm -wide “isolated defect” on the pole. Doped CH ablator material has penetrated the hot spot.

Figure 17. Simulated x-ray image (photon energy, $h\nu > 8$ keV) from the compressed core of a CH THD capsule, with a +300-nm-amplitude 20- μm -wide “isolated defect” on the pole. The high-Z jet dominates the emission from the surrounding DT plasma. The image is formed by reflecting the 90° simulation, creating two opposing jets.

Figure 18. Simulated x-ray spectra (Cretin [12]) from a THD capsule with an isolated defect, resulting from Ge-doped CH that has been injected into the hot spot.

1. Marinak, M.M., et al., *A comparison of three-dimensional multimode hydrodynamic instability growth on various National Ignition Facility capsule designs with HYDRA simulations*. Physics of Plasmas, 1998. **5**(4): p. 1125-1132.
2. Hammel, B.A., et al., *Simulations of high-mode Rayleigh-Taylor growth in NIF ignition capsules*. Journal of Physics: Conference Series, 2008. **112**(2): p. 022007 (4 pp.)-022007 (4 pp.).
3. More, R.M., et al., *A New Quotidian Equation of State (Qeos) for Hot Dense Matter*. Physics of Fluids, 1988. **31**(10): p. 3059-3078.
4. Young, D.A. and E.M. Corey, *A New Global Equation of State Model for Hot, Dense Matter*. Journal of Applied Physics, 1995. **78**(6): p. 3748-3755.
5. Wilson, B., et al., *PURGATORIO - a new implementation of the INFERNO algorithm*. Journal of Quantitative Spectroscopy & Radiative Transfer, 2006. **99**(1-3): p. 658-679.
6. Sterne, P.A., Private Communication, 2009.
7. Haan, S.W., et al., *Increasing robustness of indirect drive capsule designs against short wavelength hydrodynamic instabilities*. Physics of Plasmas, 2005. **12**(5): p. -.
8. Lee, Y.T. and R.M. More, *An Electron Conductivity Model for Dense-Plasmas*. Physics of Fluids, 1984. **27**(5): p. 1273-1286.
9. Sterne, P.A., et al., High Energy Density Physics, 2007. **3**: p. 5.
10. Edwards, J., et al., *The effects of fill tubes on the hydrodynamics of ignition targets and prospects for ignition*. Physics of Plasmas, 2005. **12**(5): p. -.
11. Hammel, B.A., *The NIF ignition program: progress and planning*. Plasma Physics and Controlled Fusion, 2006. **48**(12B): p. B497-B506.
12. Scott, H.A., *Cretin - a radiative transfer capability for laboratory plasmas*. Journal of Quantitative Spectroscopy & Radiative Transfer, 2001. **71**(2-6): p. 689-701.

¹ The CH LEOS tables were constructed using the models in [3] and [4] with cold-curve corrections to represent dissociation under compression. The Be LEOS table is also based on these references, but it uses an average-atom approximation instead of Thomas-Fermi to represent the electron-thermal contribution [5]. [6]

² In “Low Foot” case, x-ray flux in the foot (resulting from the initial “picket” in the laser pulse) was lower than “High Foot” case by a factor of 0.48, and the rest of the pulse was identical, but delayed by 1.7 ns.

³The roughness of the capsule and DT ice surfaces is specified by a random sum of modes with amplitudes expressed as sum of Legendre Polynomials, with coefficients for mode numbers (l) greater than $l = 12$, described by the following:

Be ablator:

$$R_{lm}^{inner} = \left\{ 320/l^{2.3} + \frac{0.085}{\left[(l/60)^{0.87} + (l/1200)^{3.5} \right]} \right\}; \quad R_{lm}^{outer} = \left\{ \frac{0.5}{\left[(l/70)^{0.75} + (l/700)^{3.5} \right]} \right\}$$

CH ablator:

$$R_{lm}^{inner} = \left\{ 300/l^{2.3} + \frac{0.06}{\left[(l/70)^{0.6} + (l/1200)^{3.5} \right]} \right\}; \quad R_{lm}^{outer} = 90/l^{2.3} + \left\{ \frac{0.20}{\left[(l/70)^{0.60} + (l/1200)^{3.5} \right]} \right\}$$

DT ice inner surface:

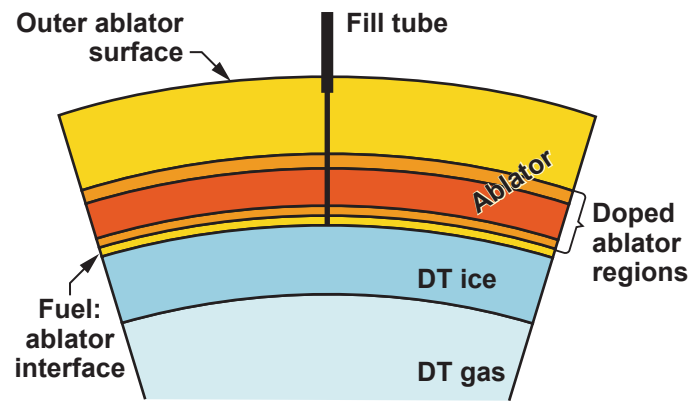
$$R_{lm}^{ice} = 2.0 * 0.87 / l^{1.1}$$

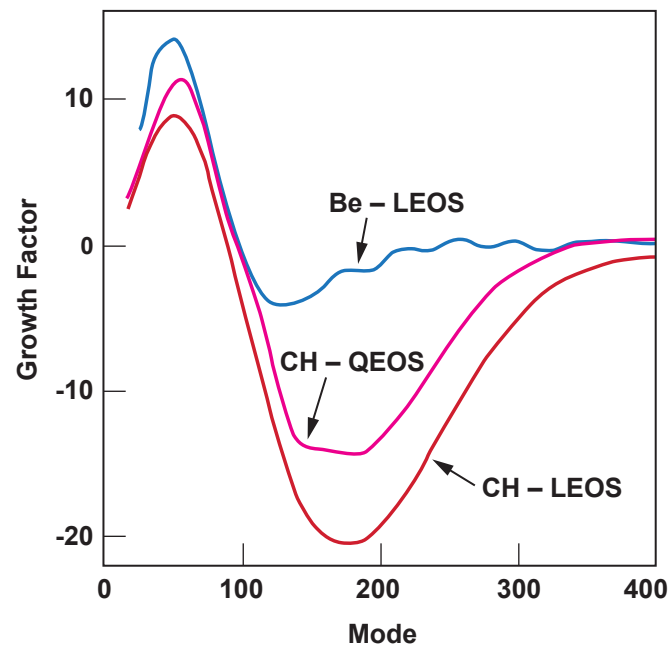
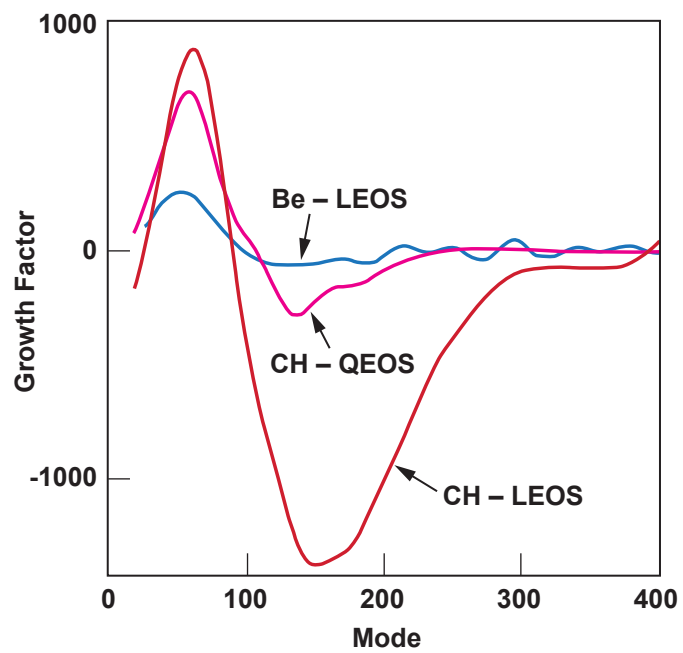
⁴ Capsule implosion velocity, fuel entropy, and low-mode perturbations of the hot-spot are each characterized by a probability distribution function (PDF) around their expected values. These PDFs flow down from, and are consistent with, the probability of variations in the experimental conditions (e.g. laser energy and power, drive symmetry, capsule and fuel dimensions, surface roughness, etc.).

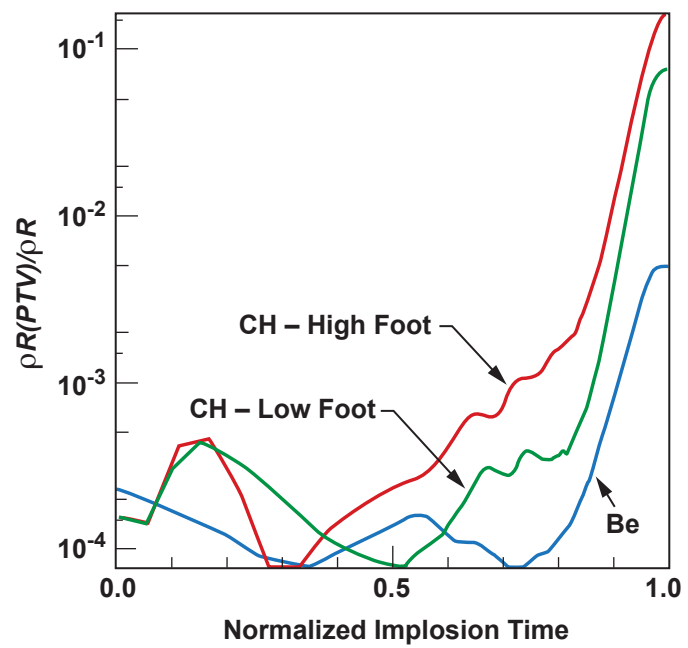
⁵ The fuel:ablator density increases over the course of the implosion, but generally reaches a approximately constant value just before peak velocity. We evaluate the ratio at this time. After, the ratio rises quickly when the density (at the position of the right triangle) begins to decrease due to ablation.

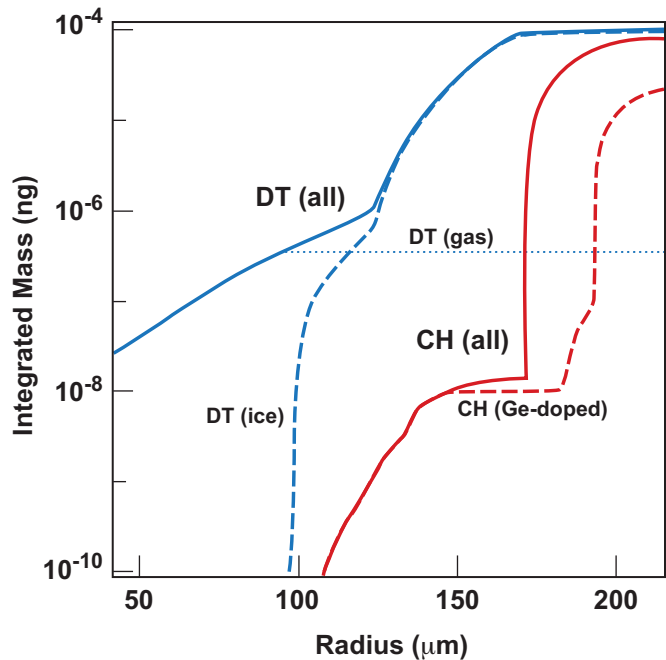
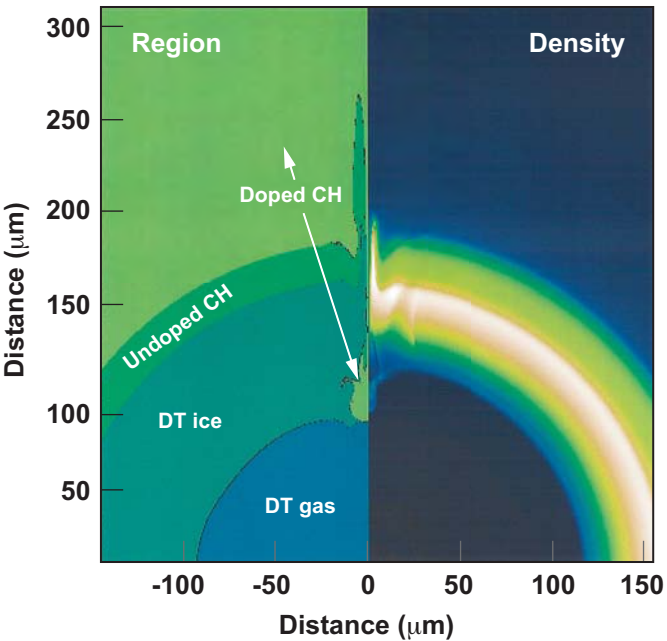
⁶ When quoting the amount of mix penetration, we refer to the amount of DT fuel that contains $\geq 10\%$ ablator material by mass.

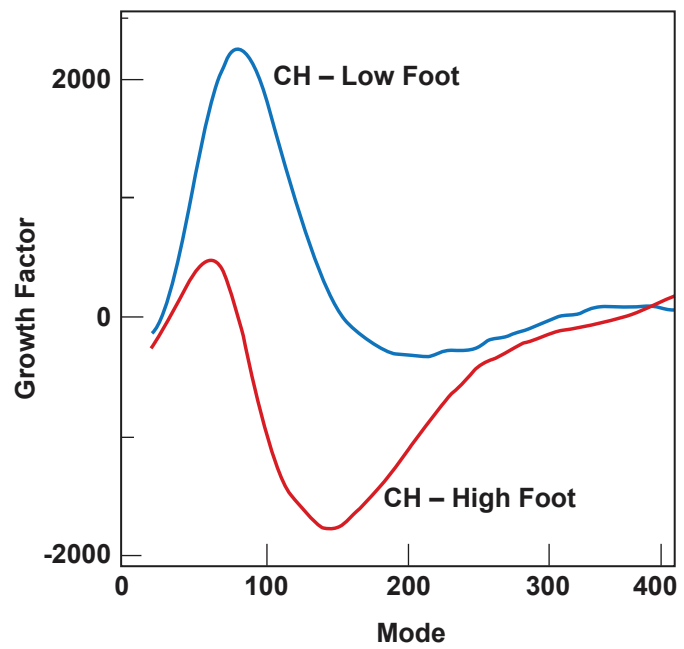
⁷ Overall estimated uncertainty in mix width is made up of: (1) 50% due to uncertainty in the amount of ablator remaining at peak velocity; (2) 40% due to uncertainty in EOS; (3) 25% due to uncertainty in thermal conductivity; (4) 25% due to uncertainty in hydrodynamic modeling; (5) 25% due to uncertainty in x-ray drive spectrum, after measurements are made in early NIF experiments.

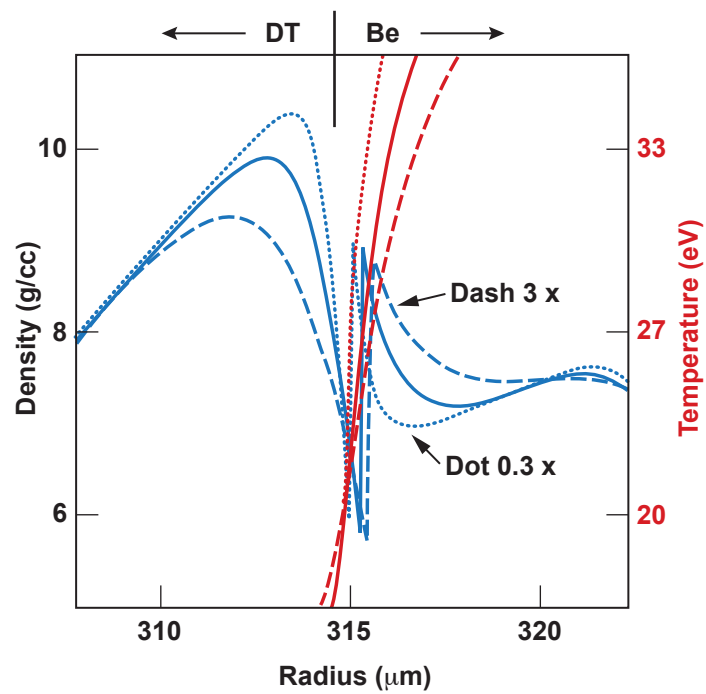
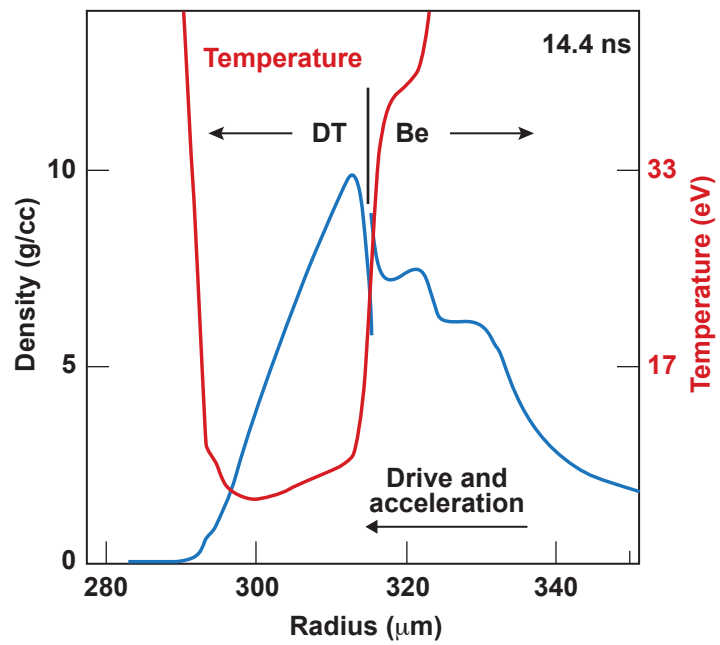


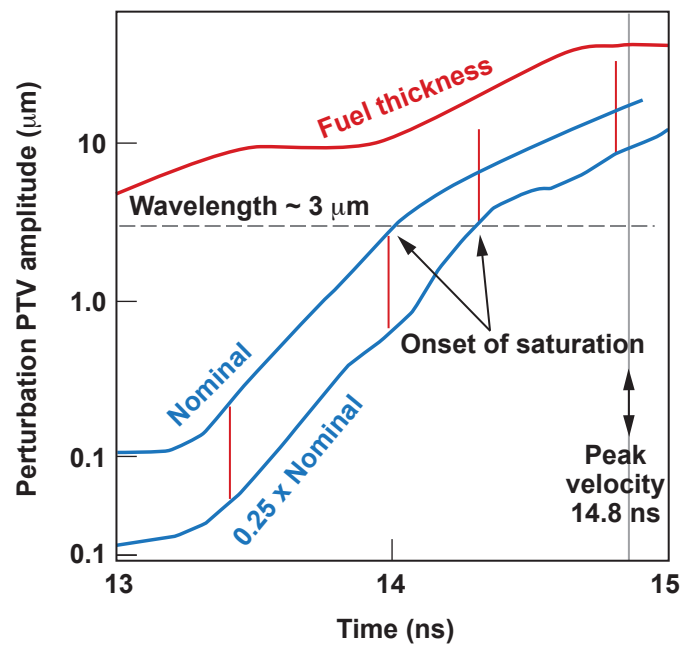
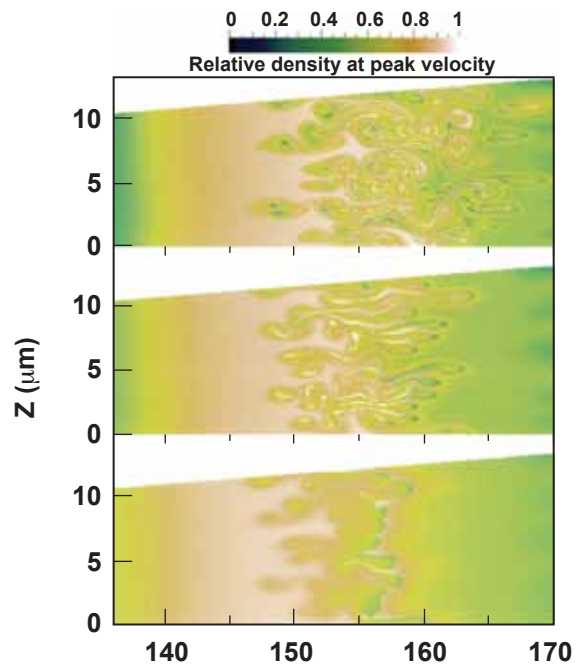


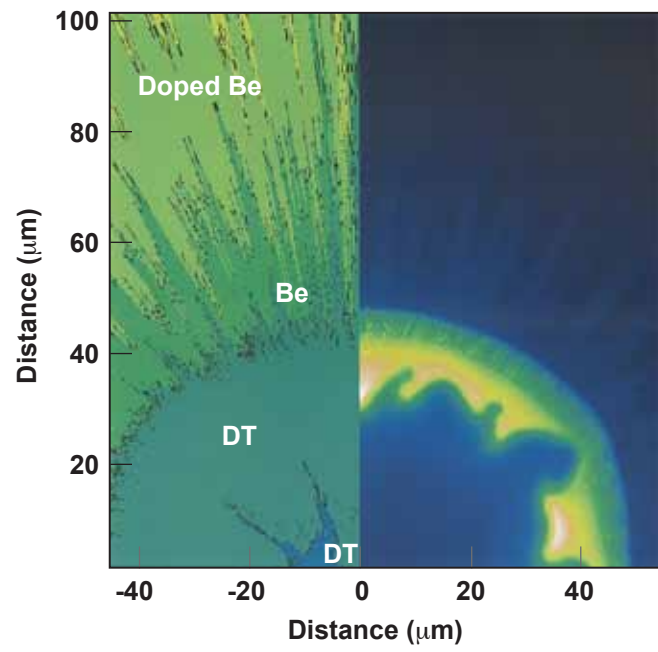


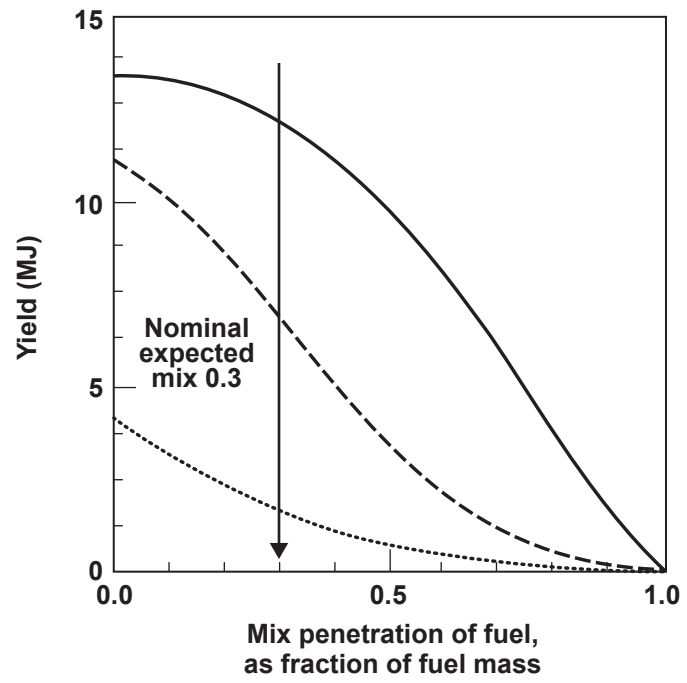


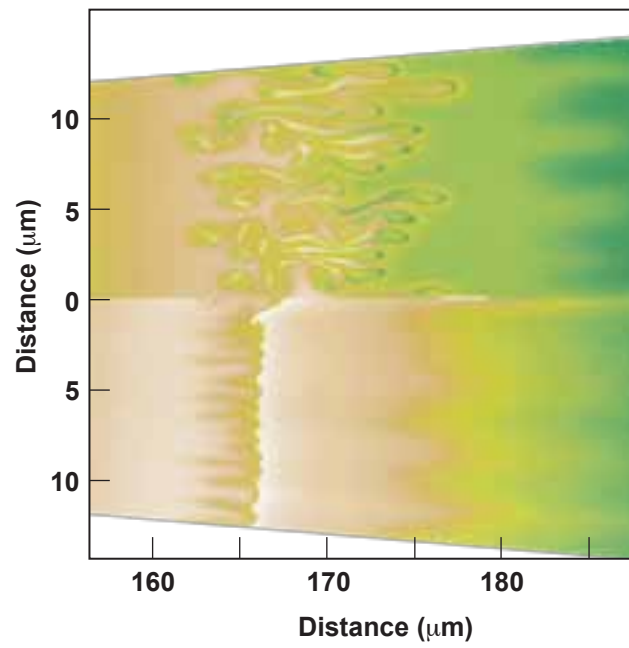
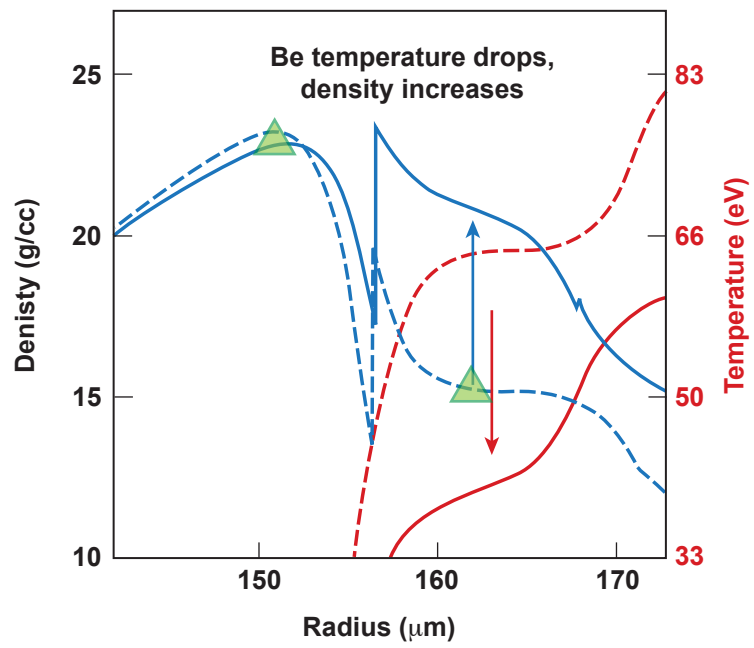


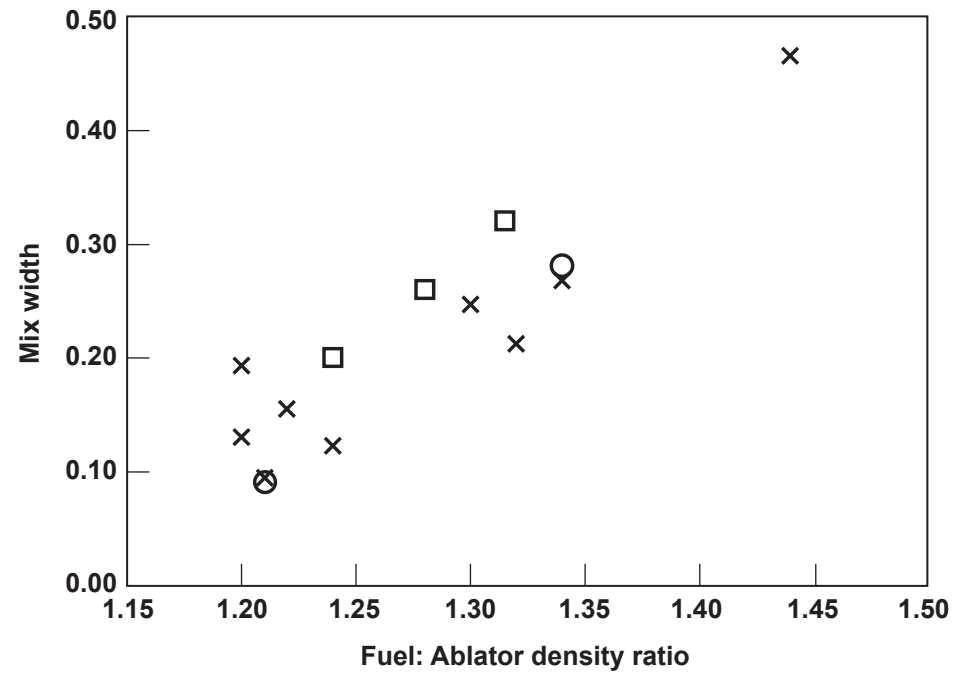


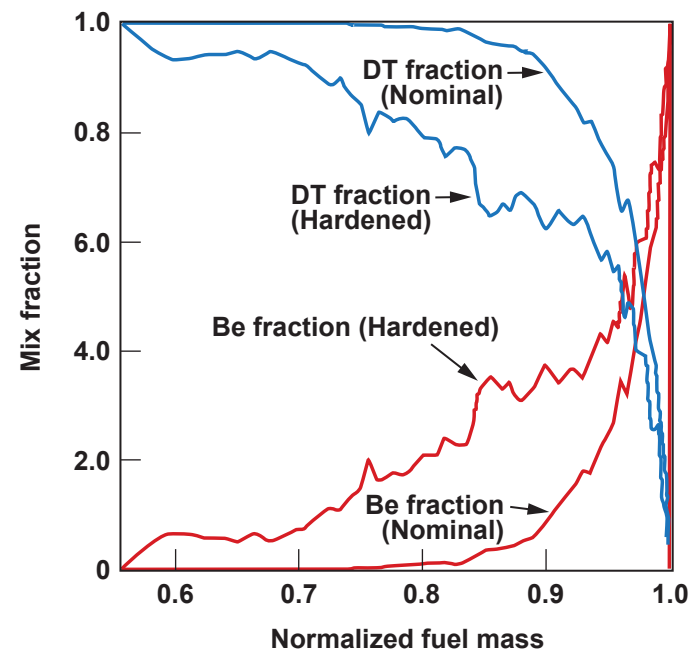
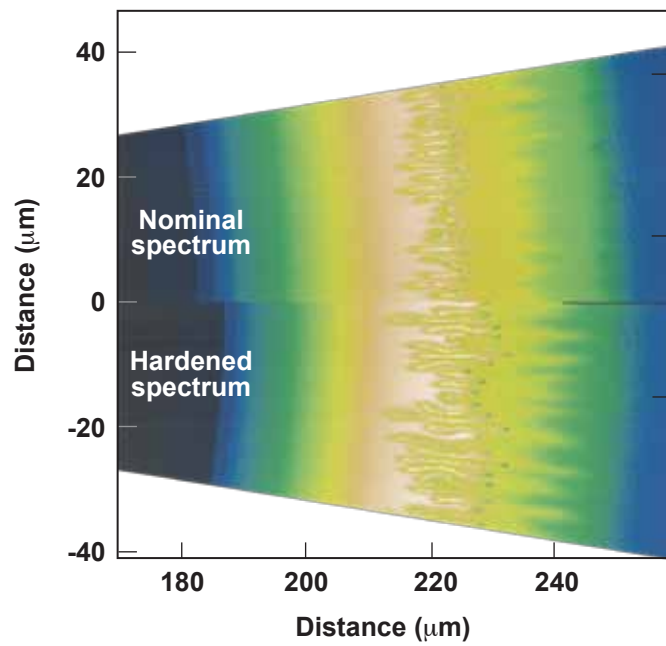


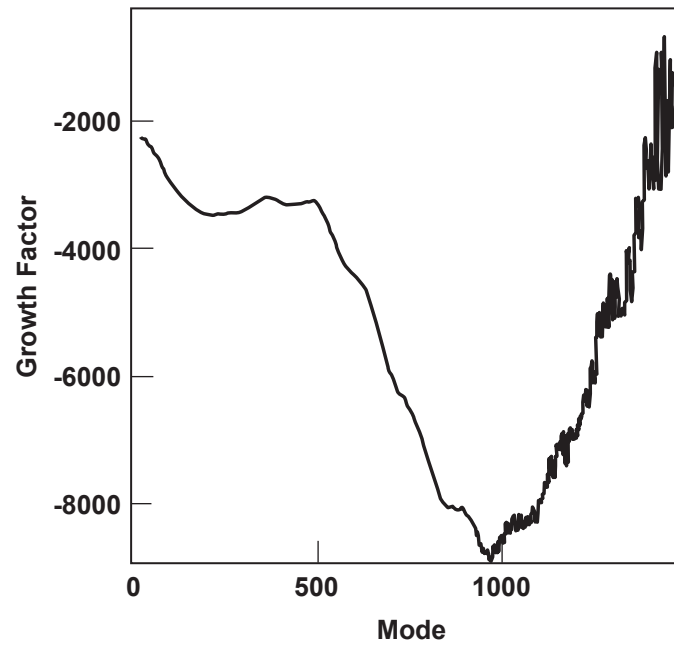


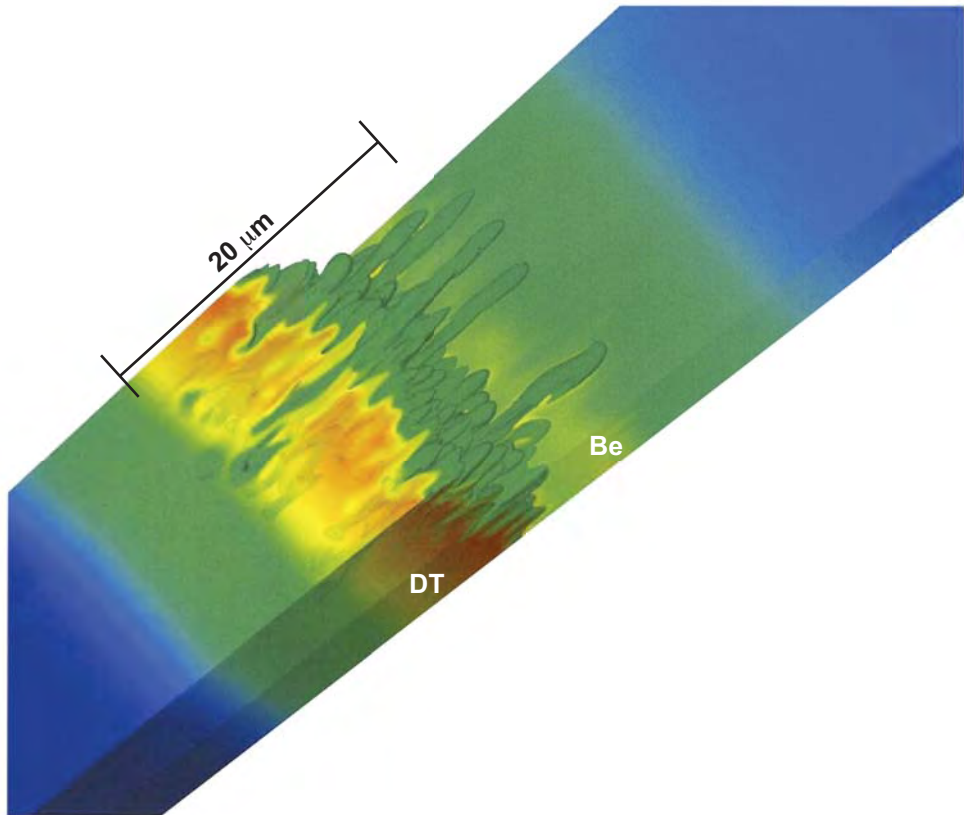












$20\ \mu\text{m}$

DT

Be

